JOURNAL OF THE KOREAN METEOROLOGICAL SOCIETY, 42, 2, 2006, p. 129-151

The WRF Single-Moment 6-Class Microphysics Scheme (WSM6)

Song-You Hong and Jeong-Ock Jade Lim*

Global Environment Laboratory, Department of Atmospheric Sciences, Yonsei University, Seoul, Korea
(Manuscript received 5 April 2006; in final form 28 April 2006)

Abstract

This study examines the performance of the Weather Research and Forecasting (WRF)-Single-Moment- Microphysics scheme (WSMMPs) with a revised ice-microphysics of the Hong *et al.* In addition to the simple (WRF Single-Moment 3-class Microphysics scheme; WSM3) and mixed-phase (WRF Single-Moment 5-class Microphysics scheme; WSM5) schemes of the Hong *et al.*, a more complex scheme with the inclusion of graupel as another predictive variable (WRF Single-Moment 6-class Microphysics scheme; WSM6) was developed. The characteristics of the three categories of WSMMPs were examined for an idealized storm case and a heavy rainfall event over Korea. In an idealized thunderstorm simulation, the overall evolutionary features of the storm are not sensitive to the number of hydrometeors in the WSMMPs; however, the evolution of surface precipitation is significantly influenced by the complexity in microphysics. A simulation experiment for a heavy rainfall event indicated that the evolution of the simulated precipitation with the inclusion of graupel (WSM6) is similar to that from the simple (WSM3) and mixed-phase (WSM5) microphysics in a low-resolution grid; however, in a high-resolution grid, the amount of rainfall increases and the peak intensity becomes stronger as the number of hydrometeors increases.

Key words: Cloud scheme, Cloud microphysics, WRF, WSM6, Numerical weather prediction, Heavy rainfall, Thunderstorm

1. Introduction

Bulk parameterization of cloud particles and precipitation drops that is primarily based on the works of Lin *et al.* (1983) and Rutledge and Hobbs (1983) has been a central feature in the representation of cloud and precipitation processes in both general circulation models and mesoscale models. For the last two decades, they have been successfully applied to the simulation of convective systems. On the other hand, some problems have been reported, for example, the production of excessive ice crystals in the upper troposphere.

Recently, Hong *et al.* (2004, hereafter HDC) suggested a revised approach to ice-microphysical processes in order to overcome the limitations identified by previous studies. The improved microphysics in their approach includes processes such as number concentration, accretion, and ice nucleation resulting in a more realistic formation of cloud ice. The most distinguishing features of this approach are that (1) it practically represents ice microphysical processes by assuming the ice nuclei number concentration to be a function of temperature and (2) it involves the new assumption that the ice crystal number concentrations are a function of the amount of ice. Relevant changes in ice microphysics have been introduced.

HDC implemented the revised ice microphysics into the Weather Research and Forecasting (WRF) model, and the performance of the model was evaluated. Thus, it is called as the WRF-Single-Moment-Microphysics scheme (WSMMPs). HDC evaluated two categories of the WSMMPs, namely, (1) class 3 (WSM3) with the prognostic water substance variables of water vapor, cloud water/ice, and rain/snow and (2) class 5 (WSM5) with water vapor, cloud, ice, rain, and snow. They concluded that together with the

Corresponding Author: Song-You Hong, Department of Atmospheric Sciences, College of Sciences, Yonsei University, Seoul 120-749, Korea.
Phone : +82-2-2123-2679, Fax : +82-2-365-5163
E-mail: shong@yonsei.ac.kr
*Current affiliation: Numerical Weather Prediction Division, Korea Meteorological Administration, Seoul, Korea

sedimentation of cloud ice, the new microphysics scheme reveals a significant improvement in the high cloud amount, surface precipitation, and large-scale mean temperature through a better representation of the ice-cloud/radiation feedback.

Lim and Hong (2005) implemented the WSM5 scheme into the fifth-generation Pennsylvania State University—National Center for Atmospheric Research Mesoscale Model (MM5). They showed that for a locally developed heavy rainfall event over Korea, the impact of the revised ice microphysics scheme is significant, whereas ice sedimentation is more important for those cases of heavy rainfall that are associated with a mobile surface cyclone system. They also found that the sedimentation of cloud ice is crucial to the successful simulation of monsoonal precipitation and large-scale features within the East Asian summer monsoon.

This study further examines the performance of the WSMMPs. In addition to simple (WSM3) and mixed-phase (WSM5) schemes of HDC, a more complex scheme (WSM6) has been developed; this scheme includes graupel as another predictive variable. The performance of the three categories of the WSMMPs, that is, the WSM3, WSM5, and WSM6 schemes, will be examined for an idealized storm case and a mesoscale convective system over Korea. Section 2 describes the development of the WSM6 scheme. Section 3 outlines the numerical experiments conducted in this study, and section 4 presents their results. Concluding remarks appear in the final section.

2. Development of the WSM6 Scheme

a. Parameterizations

The WSM6 scheme has been developed by adding additional processes related to graupel to the WSM5 scheme. In this scheme, new terms related to graupel are based on the reports of Lin *et al.* (1983) and Rutledge and Hobbs (1984). The prognostic water substance variables in this scheme include the mixing ratios of water vapor (q_V), cloud water (q_C), cloud ice (q_I), snow (q_S), rain (q_R), and graupel (q_G). The microphysical properties in the WSM6

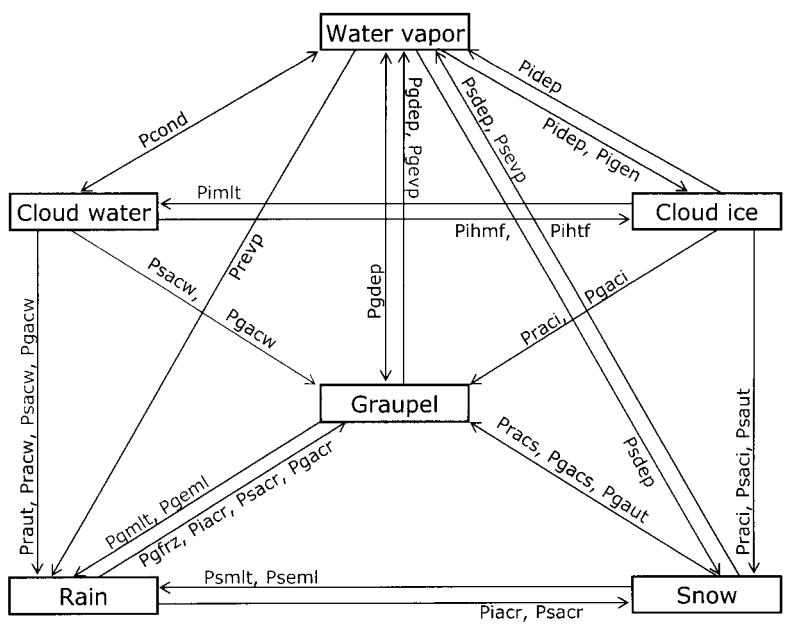

Fig. 1. Flowchart of the microphysics processes in the WSM6 scheme. The terms with red (blue) colors are activated when the temperature is above (below) 0 °C, whereas the terms with black color are in the entire regime of temperature.

scheme are demonstrated in Fig. 1. Each source/sink term in Fig. 1 is described in Appendix A, and the list of symbols is provided in Appendix B.

It is assumed that the particles comprising graupel (q_g) follow the following exponential size distribution:

$$n_G(D)dD_G[\mathrm{m}^{-4}] = n_{0G}\exp(-\lambda_G D_G)dD_G, \qquad (1)$$

where $n_G(D)dD_G(\mathrm{m}^{-4})$ is the number of graupel particles per cubic meter of air with diameters between D_G and $D_G + dD_G$; $n_{0G}(\mathrm{m}^{-4})$, the intercept values; and $\lambda_G(\mathrm{m}^{-1})$, the slope of the distribution. This slope is given by

$$\lambda_G[\mathrm{m}^{-1}] = \left(\frac{\pi\rho_G n_{0G}}{\rho q_G}\right)^{0.25}, \qquad (2)$$

where ρ_G is the density of graupel. The slope parameter can be determined by multiplying (1) by the drop mass ($=\pi\rho_G D_G^3/6$), integrating over all diameters, and equating the resulting quantities to the appropriate water contents ($=\rho q_G$). In this study, we assumed that $n_{0G} = 4\times10^6\ \mathrm{m}^{-4}$ based on the study by Houze *et al.* (1979).

The terminal velocity for a graupel particle of diameter D_G is expressed as

$$V_{DG}[\mathrm{ms}^{-1}] = a_G D_G^{b_G}\left(\frac{\rho_0}{\rho}\right)^{\frac{1}{2}}, \qquad (3)$$

which was determined by Locatelli and Hobbs (1974).

Following the reports of Lin *et al.* (1983) and Rutledge and Hobbs (1984), the mass-weighted mean terminal velocity can be obtained by integrating (3), and it is expressed as

$$V_G[\mathrm{ms}^{-1}] = \frac{a_G\Gamma(4+b_G)}{6}\left(\frac{\rho_o}{\rho}\right)^{\frac{1}{2}}\frac{1}{\lambda_G^{b_G}}. \qquad (4)$$

The continuity equation for graupel is

$$\frac{\partial q_G}{\partial t} = -\vec{V}\nabla_3 q_G - \frac{q_G}{\rho}\frac{\partial}{\partial z}(\rho V_G) + S_G, \qquad (5)$$

where the 1st and 2nd terms in the r.h.s. represent the 3D advection and sedimentation of graupel, respectively. The term S_G represents the sources and sinks of graupel.

b. Computational procedures

In the WSMMPs including the WSM6 scheme, the sedimentation of falling hydrometeors is computed before the microphysical processes, whereas the code in other microphysics schemes (e.g., Dudhia 1989) computes the microphysics first. For numerical stability, a fall-term sub-step for each model column is applied on computing the fallout terms, so that precipitate does not cross over more than one vertical level within a single loop of the calculation. A second-type of splitting approach of Hong *et al.* (1998) is applied for the microphysical processes, with a time step of 120 s for the calculation of all source and sink terms in microphysics when the model time step is greater than 120 s. The freezing/ melting processes are computed during the fall-term sub-steps to increase accuracy in the vertical heating profile of these processes. Among the microphysics terms, condensation is computed last to make sure that any supersaturated water vapor does not pass to the dynamical process.

From the sensitivity experiments of the simulated rainfall (Lim 2004), that is the same heavy rainfall event in this study, to the order of calculation of terms inside the cloud microphysics schemes for different time intervals of microphysical processes, it was found that the results with 120 s time step reasonably agree with that with 10 s time step, which is considered close to ideal, when the sedimentation of falling hydrometeors is computed first, together with the computation of melting of snow and graupel inside the sedimentation loop. Considering the stability of the model run, it seems realistic that the terms causing large changes should be placed at beginning stage of computing just after dynamical processes, and sedimentation causes larger changes than microphysical

processes do.

3. Numerical Experimental Setup

The Advanced Research WRF (ARW; Skamarock *et al.*, 2005) is a community model suitable for both research and forecasting. This model is well suited for idealized types of simulations to study baroclinic waves, idealized storm dynamics, or topographically induced flows as well as for detailed NWP cases with real-data initial states and boundary conditions. The model used in this study is the WRF version 2.1.2, which was released in January 2006. Two sets of experiments were carried out using an idealized 2D thunderstorm case and a 3D real-data simulation of a heavy rainfall event over Korea.

a. Idealized thunderstorm experiment

The idealized thunderstorm experiment was designed to systematically distinguish the intrinsic differences between the WSMMPs by the virtue of fixed initial conditions and the absence of other non-microphysical processes, which in turn would help us to understand the impact of the changes in the microphysics in the 3D framework. In the idealized experiments, other physical processes are turned off.

The idealized thunderstorm simulation is a preset option for the WRF model. We chose a 2D domain in the x direction. The grid in this direction comprised 201 points with a 250-m grid spacing. The number of vertical layers was 80. The model was integrated for 60 min with a time step of 3 s. The initial condition included a warm bubble with a 4-km radius and a maximum perturbation of 3 K at the center of the domain. A wind with a velocity of 12 m s^{-1} was applied in the positive x direction at the surface; its velocity decreased to zero at 2.5 km above the ground, with no wind above. Open boundary conditions were applied, and there was no Coriolis force or friction. The only physical parameterization was the microphysics scheme. This experiment served to demonstrate the microphysics in a quasi-steady state that simplifies the interpretation of the results.

b. Heavy rainfall experiment

A significant amount of precipitation was recorded in Korea on July 15, 2001, with a local maximum of approximately 371.5 mm near Seoul (Fig. 2a). Most of the rainfall was observed during the 12-h period from 1200 UTC July 14 to 0000 UTC July 15, 2001, and the maximum rainfall intensity was 99.5 mmh^{-1} (Fig. 2b). At 0000 UTC July 14, 2001 (not shown), there was a low-pressure system centered at the Yangtze River, with a warm front to the east and a cold front to the southwest. To the north of it, high-pressure systems extended from Manchuria to Siberia. Meanwhile, a subtropical high was present over Japan. After 12 h (Fig. 2c), the low-pressure system traveled northeastward over the Yellow Sea. This was 3 h prior to the onset of heavy rainfall over Seoul, Korea. During the heavy precipitation, the high-pressure systems located on the northern side of the peninsula prevented the monsoon front from moving northward, restricting it to Korea. Associated with this low-pressure system, convective activity was visible both to the south of the cold front and to the north of the warm front (Fig. 2d).

In association with the significant rainfall over Korea, the upper level large-scale features (not shown) indicated the strengthening of the southerly low-level jet (LLJ) bringing moisture northward to the heavy precipitation region and the intensification of baroclinicity in the mid-troposphere. The heavy precipitation region was located south of the exit of the upper-level jet. A more detailed synoptic overview related to this case is available in the report by Lim and Hong (2005).

In this study, the physics packages other than the microphysics include the Kain-Fritsch (1993) cumulus parameterization scheme, the Noah land-surface model (Chen and Dudhia, 2001), the Yonsei University planetary boundary layer (PBL) (Hong *et al.*, 2006), a simple cloud-interactive radiation scheme (Dudhia, 1989), and Rapid Radiative Transfer Model (RRTM) longwave radiation (Mlawer *et al.*, 1997) schemes.

The model configuration consisted of a nested domain configuration defined in the Lambert con-

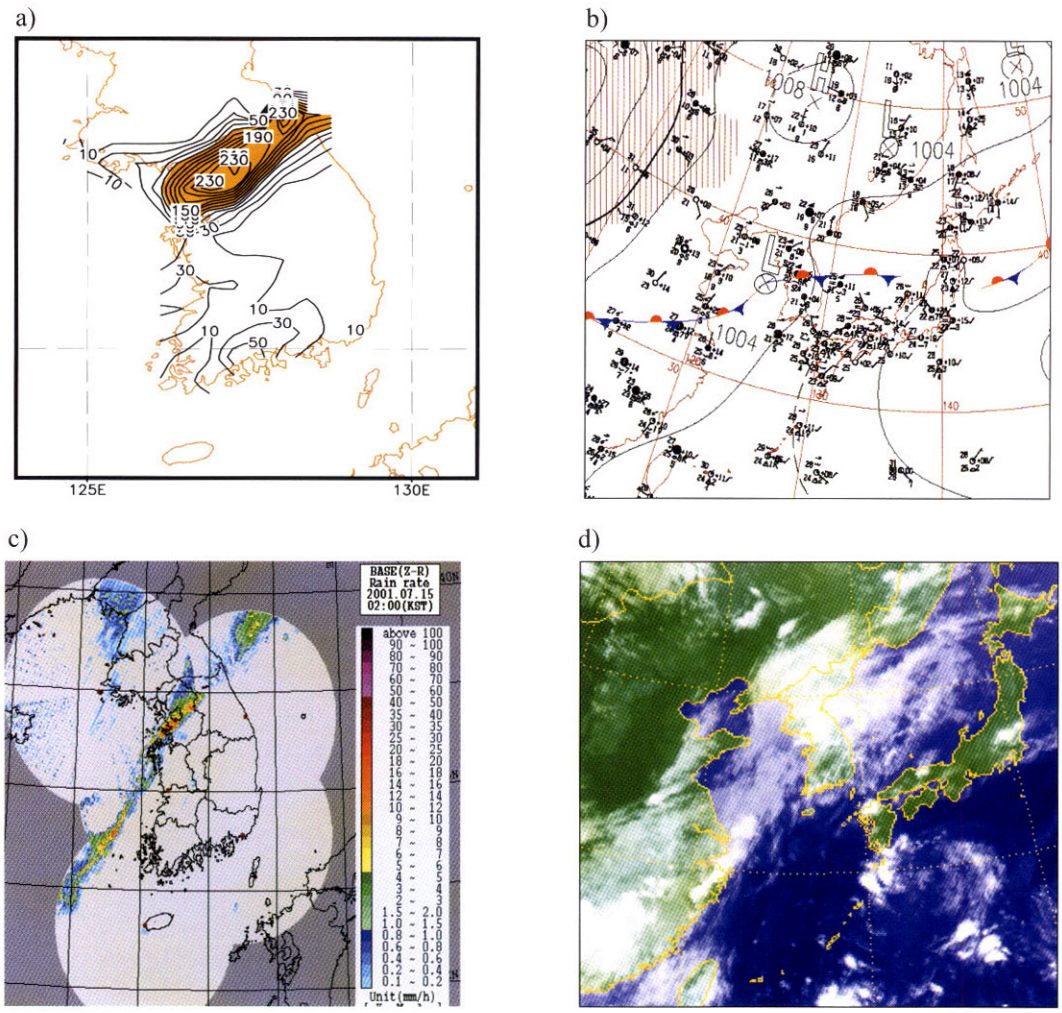

Fig. 2. (a) Observed 24-h accumulated precipitation (mm) valid at 0000 UTC 15 July 2001, (b) radar image of rain rate at 1700 UTC 14 July, (c) surface weather map analysis, and (d) satellite image at 1200 UTC 14 July 2001. Shading in figure (a) indicates where the value is over 90 (mm). All data are provided by the Korea Meteorological Administration (KMA).

formal space (Fig. 3). A 5-km model covering the Korean peninsula (Domain 3, 181 × 181), was surrounded by a 15-km grid model (Domain 2, 100 × 100), which in turn was surrounded by a 45-km grid model (Domain 1, 80 × 80) by a one-way interaction. All grid systems had 23 vertical layers and the model top was located at 50 mb. No cumulus parameterization was used at the 5-km grid model since at 5 km, updrafts may be resolved sufficiently so as to result in explicit convective vertical transports. Evaluation of the results will focused on the 45 and 5 km experiments, which are regarded to be low and high resolution grids, respectively.

Initial and boundary conditions were preprocessed through a separate package called the Standard Initialization. This was done using the global analysis and prediction system that is routinely produced at the National Centers for Environmental Prediction (NCEP) Global Data Assimilation System (GDAS). The experiments were carried out for 24 h, from 0000

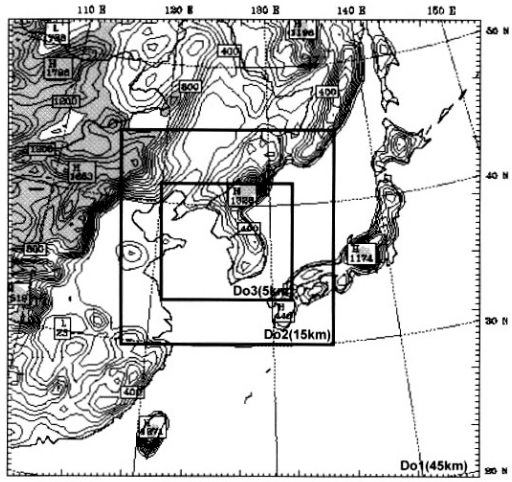

Fig. 3. Model terrain contoured every 100m for 45-km (D01). The resolutions of inner domains (D02 and D03) are 15-km and 5-km. Terrain heights greater than 1000 m are shaded.

UTC July 14 to 0000 UTC July 15, 2001.

4. Results

a. Idealized experiments

Figure 4 compares the condensate fields from the experiments with the three categories of the WSMMPs. The general structure of the thunderstorm, such as the cloud/ice water in the updraft region near the storm center and anvil clouds, was well simulated irrespective of the complexity in the microphysics. Cloud condensate reaches a maximum in the mid-troposphere in the area of the updraft in all three experiments. The overall similarity between the results from the WSM3, WSM5, and WSM6 schemes confirms that the revised ice microphysical processes of HDC are applicable even for a high reso-

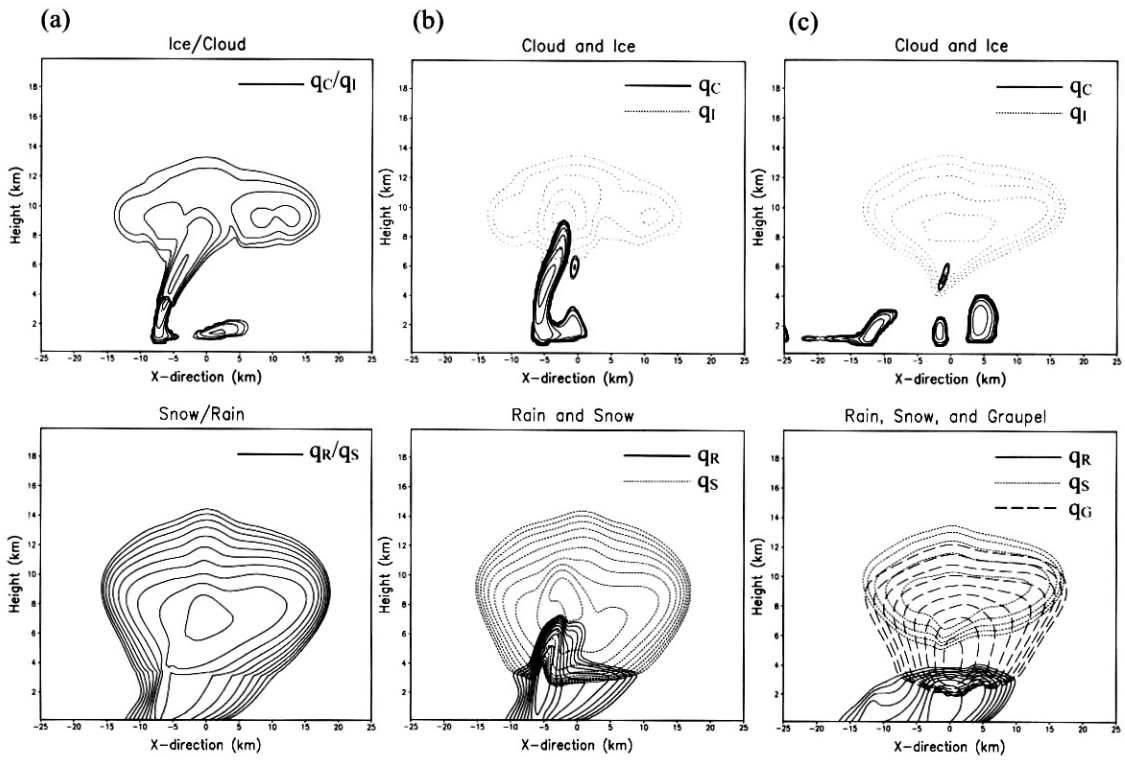

Fig. 4. Isolines of the condensation fields for cloud particles (first row) and precipitable particles (second row) from the experiments with the (a) WSM3, (b) WSM5, and (c) WSM6 schemes. Contour lines are at 0.01, 0.02, 0.04, 0.08, 0.16, 1.28, 2.56, 5.12, and 10.24 gkg^{-1}.

lution of 250 m in the horizontal grid spacing. The basic features of the simulated storm are unchanged with respect to the number of prognostic water substance variables; however, the detailed evolutionary features of the hydrometeors and the precipitation activity are affected by the complexity in the microphysics, as described below.

The time series of domain-averaged precipitation rate and hydrometeor path is plotted in Fig. 5, and the vertical profiles of time-domain-averaged condensates in Fig. 6. The hydrometeor path is defined by the vertical integral of the sum of all condensates with respect to the height ($=\int_0^{z_{top}} \rho q_{total} dz$). It can be seen that the amount of precipitation increases as the number of prognostic water substance variables increases (Fig. 5a), whereas the amount of volume-averaged water substance decreases (Fig. 5b). The WSM3 experiment shows a steady precipitation activity after 30 min. Compared to the WSM3 experiment, a stronger surface rain intensity can be observed in the WSM5 experiment, in which the maximum intensity is approximately doubled just after the 30-min integration.

These different behaviors can be attributed to the fundamental differences between the WSM3 and WSM5 schemes. A primary difference between the two schemes is that melting and freezing processes occur within a deeper layer in the WSM5 scheme, whereas they occur as instantaneous processes at the freezing level in the WSM3 scheme. The maximum updraft velocity was determined to be approximately 20 m/s at a height of 8 km at 20 min, which is enough to rapidly transport the cloud particles to the freezing level above. Thus, in the WSM5 experiment, cloud particles can penetrate deeper up to 10 km; however, the clouds were immediately converted to cloud ice above the freezing level by the WSM3 experiment (c.f. Figs. 6a and 6b). The production of rain in the WSM3 scheme is inefficient since falling snow should reach the freezing level to be converted to rain. The accretion of clouds and ice by snow is also inefficient in this scheme since water and ice phases do not coexist. Therefore, the early peak in the WSM5 scheme in Fig. 5a is found to be due to the fact that the autoconversion from clouds to rain is more efficient at producing precipitation than the ice phase alone in the WSM3 case. The accretion of clouds by snow in the WSM5 scheme, which is an additional mixed-phase process in the WSM5 scheme, would

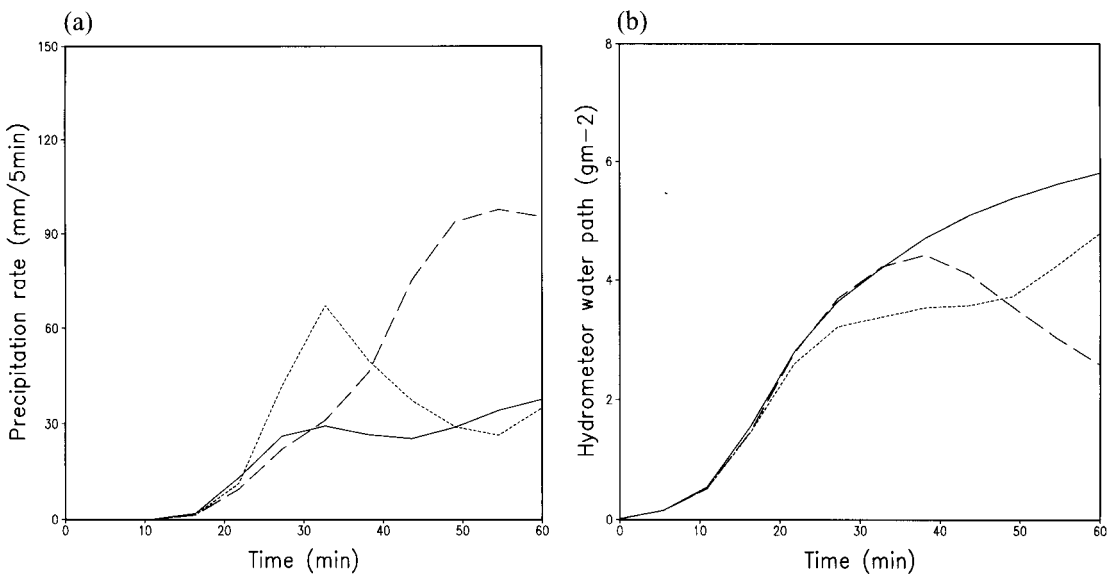

Fig. 5. Time series of the (a) surface precipitation rate (mm/5min), and (b) hydrometeor path amount, resulted from the WSM3 (solid), the WSM5 (dotted), and WSM6 (dashed) experiments over the whole domain.

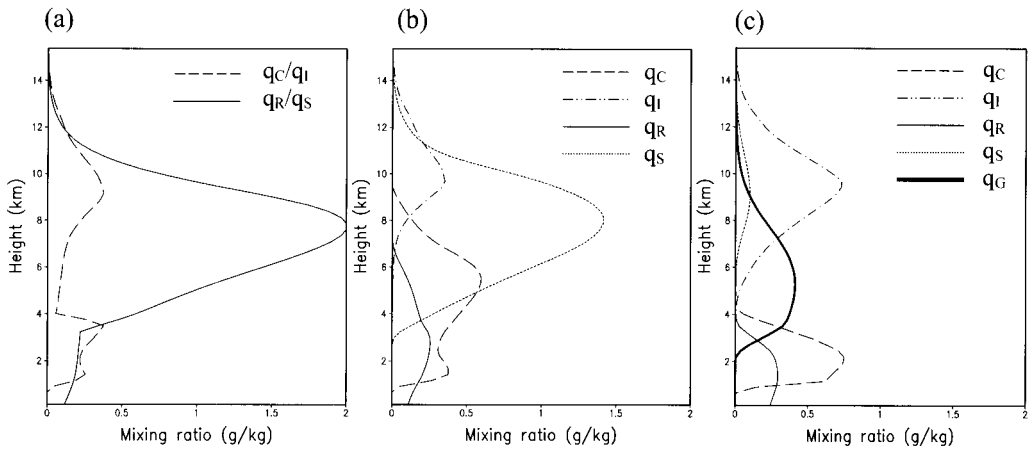

Fig. 6. Vertical distribution of the domain-averaged water species during the 60 min integration period, obtained from the (a) WSM3 (b) WSM5, and (c) WSM6 experiments. Units are gkg^{-1} for rain, snow, and graupel, and 10 gkg^{-1} for cloud ice and cloud waters.

add rainwater below the freezing level.

The precipitation intensity in the WSM5 experiment weakened with time since further cooling below 4 km would possibly occur due to more melting in the WSM5 scheme. This difference in melting might be expected to increase downward because when all the melting occurs just at the freezing level, as in the WSM3 experiment, subsidence may cause the cooling to extend downward a little. However, the effect of subsidence is limited by the stability. It was observed that in the WSM5 scheme, snow could melt even below the layer where the subsidence reaches in the WSM3 scheme; therefore, the cooling is deeper. This effect results in the reduction of the precipitation intensity after 30 min in the WSM5 scheme, as compared to that in the WSM3 scheme. To be consistent with the weakened precipitation activity, the WSM3 scheme produces more hydrometeors in the atmosphere (Fig. 5b).

A later development of surface precipitation and intense storm intensity in the WSM6 scheme as compared to in the WSM5 scheme are not simple to explain since there are several additional processes in the WSM6 scheme. A major reason for the later development of the storm in the WSM6 scheme can be attributed to the fact that the conversion of cloud particles to graupel and following melting processes are needed to produce precipitation, whereas the direct conversion from clouds to rain can produce precipitation quickly in the WSM5 scheme. A more intense surface precipitation after 30 min in the WSM6 experiment can be due to a greater accretion by graupel in the WSM6 scheme through faster sedimentation than that by snow in the WSM5 scheme. Fewer hydrometeors in the WSM6 experiment than in the WSM5 experiment indicates the faster removal of clouds and ice by graupel in the WSM6 scheme than by snow in the WSM5 scheme (Fig. 5b).

b. Heavy rainfall event

Figure 7 shows that in general, all simple ice, mixed-phase, and graupel experiments capture the observed heavy rainfall extending from southwest to northeast across the central part of the Korean peninsula; however, the maximum amount of rainfall is underestimated (c.f. Fig.2 a). At low resolutions (upper panels of Fig. 7), there are no distinct differences in precipitation due to the complexity in microphysics. At 5 km (lower panels of Fig. 7), the overall distribution of the simulated precipitation is not changed; however, the maximum amount of rainfall is greater in the WSM6, WSM5, and WSM3 schemes, in that order. These features are better ex-

plained by the instantaneous radar echoes (Fig. 8). The precipitation band becomes more localized with a stronger rainfall intensity as the complexity in microphysics is increased. The leading edge of the con-

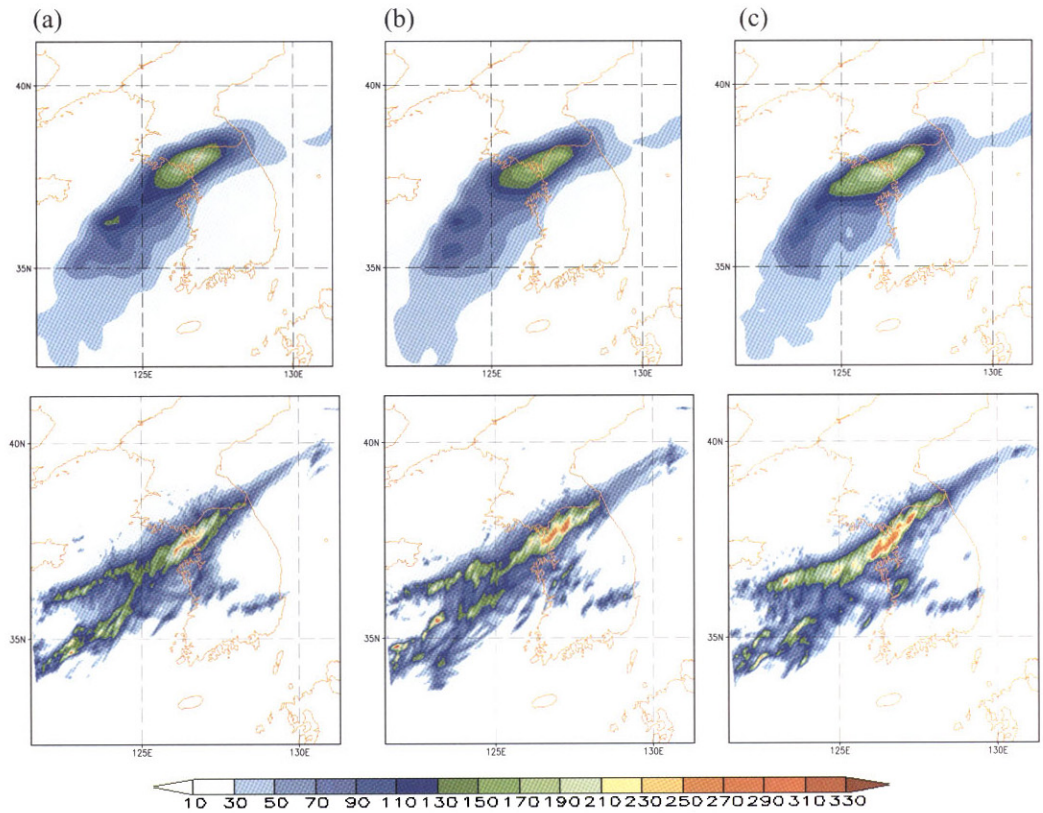

Fig. 7. 24-h accumulated rainfall (mm) ending at 0000UTC 15 July 2001, obtained from the (a) WSM3, (b) WSM5, and (c) WSM6 experiments. Upper (lower) panels are from the 45-km (5-km) resolution results.

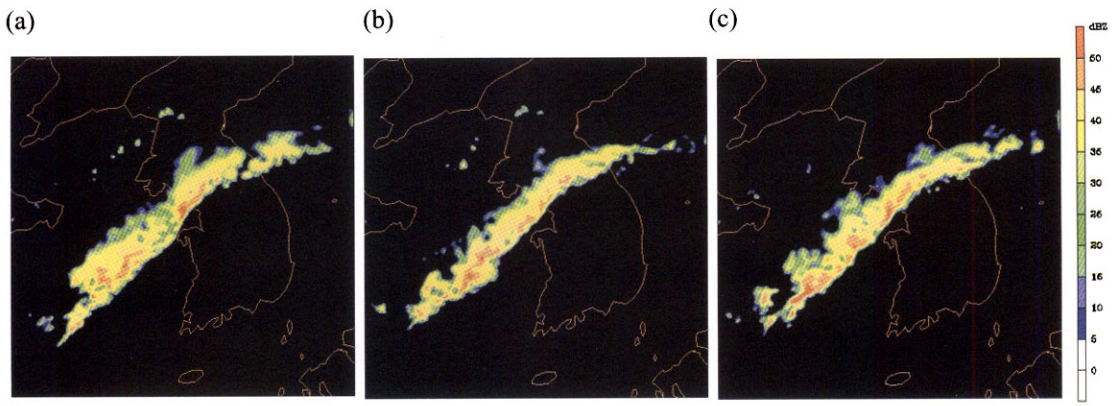

Fig. 8. Radar echo reflectivity (dBZ) at 17 UTC 14 July 2001, derived from the (a) WSM3, (b) WSM5, and (c) WSM6 experiments at the 5-km resolution.

Table 1. The pattern correlation coefficients (PC) and bias score of the 24-h accumulated precipitation over South Korea with respect to surface observation ending at 00 UTC 15 July 2001, obtained from the 45-km (5-km) resolution experiments.

	Precipitation			
	Over the Korean Peninsula			Over the whole domain
	Correlation	Bias score	Maximum (mm)	Average (mm)
WSM3	0.63(0.69)	1.67(1.45)	220(240)	21.36(20.61)
WSM5	0.70(0.71)	1.66(1.68)	195(295)	20.95(22.39)
WSM6	0.75(0.65)	1.61(1.61)	215(305)	21.22(23.14)

vection is better shaped in the WSM6, WSM5, and WSM3 schemes, in that order. These characteristics in the WSM6 scheme agrees well with the observed feature (see Fig. 2c).

Table 1 shows a comparison of the statistics of simulated precipitation over South Korea, as computed from the three microphysics schemes. The number of surface observations stations at automatic weather stations (AWS) across South Korea is 450; the horizontal resolution at these stations is approximately 15 km. Thus, the statistical skill scores are computed on the WRF grid with the 15-km grid. The observed precipitation data accumulated over 24 h are interpolated on the WRF grid by using a simple objective analysis (Cressman, 1959) to compute the statistics. The spatial pattern correlation is computed for the simulated and observed precipitation on the WRF grids for each experiment. The bias of precipitation for each experiment is the ratio of the area-averaged simulated precipitation to the observed value. Table 1 also shows that there are no systematic differences with respect to the number of hydrometeors in the low-resolution grid even though the pattern correlation improved as the complexity in the microphysics increased. However, the maximum amount of precipitation and the total amount of surface rain systematically increased with an increase in the number of hydrometeors in the high-resolution grid.

Figure 9 compares the vertical profiles of averaged condensates over the heavy rainfall region centered in Korea. As in the idealized experiment, the results of the WSM3 and WSM5 schemes produce similar profiles of rain/snow and cloud ice/water. The maximum values of the snow mixing ratio for the WSM3 and WSM5 schemes appear at 500 hPa; however,

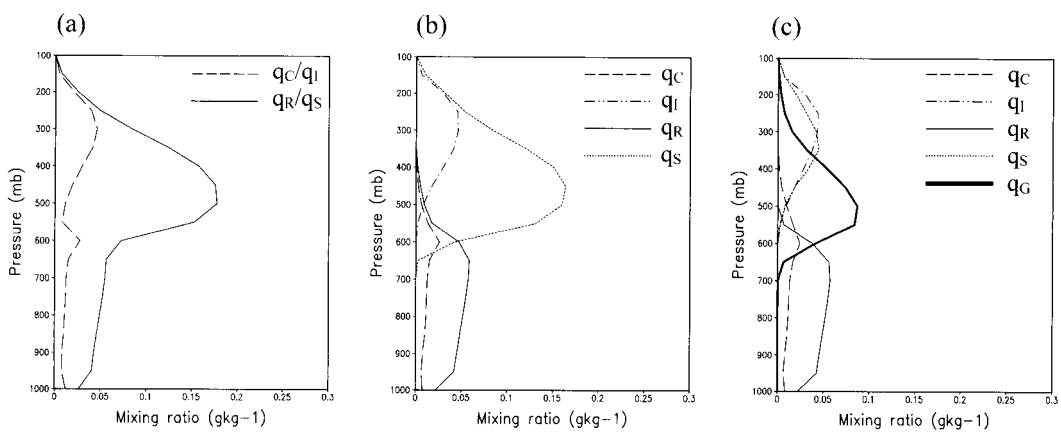

Fig. 9. Vertical distribution of water species, obtained from the (a) WSM3, (b) WSM5, and (c) WSM6 experiments, averaged over the heavy rainfall region (32.3-41.2 N, 121.5-131.3 E) during the 24-h forecast period.

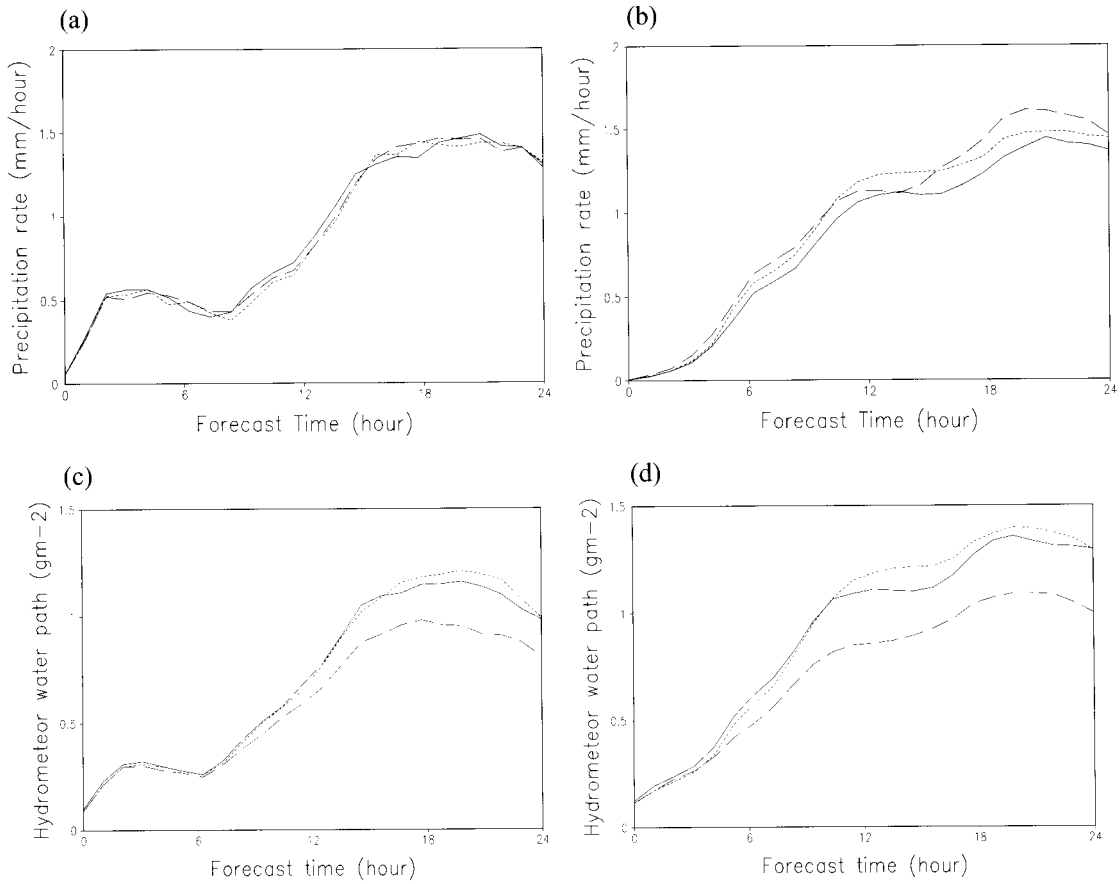

Fig. 10. Time series of the (a) surface precipitation rate and (b) hydrometeor path, resulted from the 45-km experiments with the WSM3 (solid), WSM5 (dotted), and WSM6 (dashed) schemes, averaged over the heavy rainfall region (32.3-41.2 N, 121.5-131.3 E), and the corresponding 5-km experiments, (c), and (d).

most of the snow in the WSM5 scheme is accounted for by graupel in the WSM6 scheme, as seen in the idealized experiments.

Figure 10 shows the time-series of precipitation rate and the hydrometeor path computed from the experiments using the three schemes. At 45 km (in lower resolutions), the differences in surface precipitation are not visible with respect to the categories of the prognostic water substance variable, whereas the evolution of hydrometeors shows distinct differences (Figs. 10a and b). At 5 km (in high resolutions), the amount of hydrometeors in the atmosphere is decreased in the WSM5, WSM3, and WSM6 schemes, in that order; however, the amount of precipitation is distinctly affected by the complexity in the microphysics (Figs. 10c and d).

From the comparison of Fig. 10c and 5a, it can be seen that the evolution of precipitation from the 5-km experiment (high resolution) qualitatively follows the results from the idealized runs. As analyzed in the idealized experiments, the WSM3 experiment produces a smaller amount of precipitation than the WSM5 and WSM6 schemes during the forecast period. A greater precipitation than that predicted by the WSM5 scheme till the 15-h forecast period and a stronger precipitation activity after that period than that predicted by the WSM6 scheme also comply with the results obtained in the idealized tests.

The fewer remaining hydrometeors in the atmosphere in the case of the WSM6 scheme in the high resolution partially reflects greater precipitation than that simulated by the other schemes. The amount of hydrometeors in the WSM6 experiment remains small even in the low resolution in spite of a similar amount of surface precipitation. A possible reason is that density of graupel is greater than that of snow in the WSM5 scheme, leading to a higher fall-out rate. The increase in the amount of hydrometeors is also more apparent in the WSM5 scheme than in the WSM3 scheme with time, but not significantly.

The evolution of precipitation and hydrometeors in the 5-km grid qualitatively follows the sensitivity analyses made in the idealized thunderstorm case; however, the effects are much smaller. One reason is that only the microphysical processes are activated in the 2D idealized experiment in which the interaction between the microphysics and other physical processes such as radiation is neglected. In the 3D real case experiment, the effects of microphysics are reduced since precipitation processes are influenced by all the dynamical and physical processes in the model, which are highly nonlinear. Also, another important difference between the idealized and real cases is the length of the runs. In the real case, the long simulation time probably means that the precipitation total depends mostly on the large scale moisture converging or available in the area. This is whey the totals all the similar. In the short idealized run, there is no forcing except the convection itself, and the precipitation depends mostly on the cloud dynamics, processes and local latent heating effects.

On the whole, the number of predictive hydrometeors in the WSMMPs has a negligible impact on the simulated precipitation in low resolutions, whereas in high resolutions, there are distinct differences in the amount of precipitation and its temporal evolution, with respect to the complexity in microphysics. Such a resolution dependency of the WSMMPs appears to be due to the grid-resolvable forcing that increases as the effective grid size decreases. A lower (higher) sensitivity of the complexity in the microphysics in the lower (higher) resolution grid is a beneficial aspect of the WSMMPs.

5. Concluding Remarks

This study examined the performance of the WSMMPs with a revised version of the ice microphysics proposed by HDC. In addition to simple (WSM3) and mixed-phase (WSM5) schemes of HDC, a more complex scheme that includes graupel as another predictive variable (WSM6) was developed. The characteristics of the three categories of WSMMPs were examined for an idealized storm case and a heavy rainfall event over Korea.

Based on a 2D idealized thunderstorm simulation and 3D real-case simulation of a heavy rainfall event over Korea, it was found that the number of predictive hydrometeors in the WSMMPs has a negligible impact on the simulated precipitation in low resolutions, whereas in high resolutions, there are distinct differences in the amount of precipitation and its temporal evolution, with respect to the complexity in microphysics. Such a resolution dependency of the WSMMPs confirms that the microphysics proposed by HDC behaves realistically in response to the appropriate grid-resolvable forcing.

The WSM6 scheme has been one of the options of microphysical processes in the WRF model since August 2004. This scheme has been extensively evaluated at NCAR and has demonstrated a good performance against the Purdue-Lin scheme (Chen and Sun, 2002) (Personal communications with J. Dudhia and B. Kuo). A comparison study of the WSM6 and PLIN schemes focusing on the differences in the microphysics production terms and the sedimentation velocity for graupel in the two schemes is currently being designed.

Acknowledgments. The authors would like to express their gratitude to Korea Meteorological Administration (KMA) for providing the satellite images and observed precipitation analyses. This work was funded by the Korea Meteorological Administration Research and Development Program under Grant CATER_2006-2204. A part of work has been done during the both authors visit to NCAR, which was supported partly by NCAR. We gratefully acknowledge the valuable contributions provided by

Jimy Dudhia during the development of the WSM6 scheme and its implementation onto the WRF model. Thanks go also to Matthew Gilmore and Andy Heymsfield for helpful suggestions in the early stages of this work. We are grateful to Tae-Young Lee, John Brown, Bill Kuo, and Joe Klemp for their interest and encouragement. Ju-Hye Kim, Kyo-Sun Lim, and Jung-Eun Kim helped to prepare the manuscript, which should be acknowledged.

REFERENCES

Bigg, E. K., 1953: *The supercooling of water.* Proc. Phys. Soc. London, B66, 688-694.

Chen, F., and Dudhia, J., 2001: Coupling an Advanced Land Surface-Hydrology Model with the Penn State-NCAR MM5 Modeling System. Part I: Model Implementation and Sensitivity. *Mon. Wea. Rev:*, **129,** 569-585.

Chen, S.-H., and W.-Y. Sun, 2002: A one-dimensional time dependent cloud model. *J. Meteor. Soc. Japan*, **80,** 99-118.

Cressman, G. P., 1959: An operational objective analysis system. *Mon. Wea. Rev,.* **87,** 367-374.

Dudhia, J., 1989: Numerical study of convection observed during the winter monsoon experiment using a mesoscale two-dimensional model. *J. Atmos. Sci.*, **46,** 3077-3107.

Hong, S. -Y., Y. Noh, and J. Dudhia, 2006: A new vertical diffusion package with an explicit treatment of entrainment processes. *Mon. Wea. Rev.*, in press.

_____, J. Dudhia, S.-H. Chen, 2004: A revised approach to ice-microphysical processes for the bulk parameterization of cloud and precipitation., *Mon. Wea. Rev.,* **132,** 103-120.

_____, H.-M. H. Juang, and Q. Zhao, 1998: Implementation of prognostic cloud scheme for a regional spectral model, *Mon. Wea. Rev.,* **126,** 2621-2639.

Houze, R. A., P. V. Hobbs, P. H. Herzegh and D. B. Parsons, 1979: Size distributions of precipitation particles in frontal clouds. *J. Atmos. Sci.*, **36,** 156-162.

Kain, J., and M. Fritsch,1993 : Convective parameterization for mesoscale models : The Kain-Fritsch scheme. The representation of cumulus convection in numerical models, Meteor. Mono., **24,** *Amer. Meteor. Soc.*, 165-170.

Lim, J.-O. J., 2004: The Effect of ice microphysics on the simulation of heavy rainfall. Master thesis, Yonsei University, 87 pp.

_____, and S.-Y. Hong, 2005: Effects of bulk ice microphysics on the simulated monsoonal precipitation over east Asia, *J. Geophys. Res.,* **110**(D24), 06 166-06 181.

Lin, Y.-L., R. D. Rarley, and H. D. Orville, 1983: Bulk parameterization of the snow field in a cloud model. *J. Appl. Meteor.*, **22,** 1065-1092.

Locatelli, J. D., and P. V. Hobbs, 1974: Fall speeds and masses of solid precipitation particles. *J. Geophys. Res.*, **79,** 2185-2197.

Mlawer, E. J., S. J. Taubman, P. D. Brown, M. J. Iacono, and S. A. Clough, 1997: Radiative transfer for inhomogeneous atmosphere: RRTM, a validated correlated-k model for the long wave. *J. Geophys. Res.,* **102**(D14), 16 663-16 682.

Rutledge, S. A., and P. V. Hobbs, 1983: The mesoscale and microscale structure and organization of clouds and precipitation in midlatitude cyclones. Part VIII: A model for the "seeder-feeder" process in warm-frontal rainbands. *J. Atmos. Sci.,* **40,** 1185-1206.

_____, and _____, 1984: The mesoscale and microscale structure and organization of clouds and precipitation in midlatitude cyclones. XII: A diagnostic modeling study of precipitation development in narrow cloud-frontal rainbands. *J. Atmos. Sci.,* **20,** 2949-2972.

Skamarock, W. C., J. B. Klemp, J. Dudhia, D. O. Gill, D. M. Barker, W. Wang and J. G. Powers, 2005: A Description of the Advanced Research WRF Version 2. NCAR technical note, NCAR/TN-468+STR.

Tripoli, G. J., and W. R. Cotton, 1980: A numerical investigation of several factors contributing to the observed variable intensity of deep convection over south Florida. *J. Appl. Meteor.*, **19,** 1037-1063.

Yau, M. K., and P. M. Austin, 1979: A model for hydrometeor growth and evolution of raindrop size spectra in cumulus cells. *J. Atmos. Sci.,* **36,** 655-668.

Final complete manuscript : 29 April, 2006

Appendix A. Microphysics in WSM6

The WSM6 microphysics scheme is an extension of the WSM5 scheme, which is based on the revised ice-microphysics suggested by HDC. A theoretical background and its characteristics of the ice-microphysics in the WSMMPs are described in HDC. The addition of graupel substance in the WSM6 closely follows that of Lin *et al.* (1983) and Rutledge and Hobbs (1984). For completeness, each production term for graupel, snow, rain, cloud water, and cloud ice will be discussed below. Readers are to refer HDC, Lin *et al.* (1983) and Rutledge and Hobbs (1984) for a more detailed description of each production term, and the references therein. All symbols are explained in Appendix B. All units are in M.K.S.

a. Production term for graupel

The production term for graupel may be written for two temperature regimes.

(i) If the temperature is below 0 °C ($T < T_0$):

$$\begin{aligned} S_g=&\text{Pgaut}+\text{Piacr}(1-\delta_3)+\text{Praci}(1-\delta_3)\\ &+\text{Pracs}(1-\delta_2)+\text{Psacr}(1-\delta_2)+\text{Pgaci}\\ &+\text{Pgacw}+\text{Pgacr}+\text{Pgacs}+\text{Psacw}+\text{Pgdep}\\ &+\text{Pgfrz}, \end{aligned} \tag{A1}$$

where

$$\delta_2=\begin{cases}1, (q_R \text{ and } q_s < 10^{-4}\,\text{kgkg}^{-1})\\ 0, \text{otherwise}\end{cases} \tag{A2}$$

and

$$\delta_3=\begin{cases}1, (q_R < 10^{-4}\,\text{kgkg}^{-1})\\ 0, \text{otherwise}.\end{cases}$$

(ii) If the temperature is above 0 °C ($T \geq T_0$):

$$S_g=\text{Pgacs}+\text{Pgmlt}+\text{Pgeml}+\text{Pgevp}. \tag{A4}$$

1) AGGREGATION (Pgaut)

The aggregation rate can be expressed as

$$\text{Pgaut}[\text{kgkg}^{-1}\text{s}^{-1}]=\alpha_2(q_S-q_{S0})/\Delta t. \tag{A4}$$

2) ACCRETION (Praci, Psacw, Pgacw, Pgaci, Psacr, Pracs, Pgacr, Pgacs, Piacr)

Graupel grows by accretion of other species, such as cloud water, cloud ice, rain and snow. The collection of cloud water by graupel is assumed to follow the continuous collection equation, which can be expressed as

$$\begin{aligned} &\int_0^\infty \frac{dM(D_G)}{dt}dD_G[\text{kgm}^{-3}\text{s}^{-1}]\\ &=\int_0^\infty \frac{\pi}{4}\rho D_G^2 a_G (D_G^{b_G})\left(\frac{\rho_0}{\rho}\right)^{1/2} q_c E_{GC} n_{0G}\exp(-\lambda_G D_G)dD_G\\ &=\frac{\pi a_G E_{GC} n_{0G} q_C \rho}{4}\left(\frac{\rho_0}{\rho}\right)^{1/2}\frac{\Gamma(3+b_G)}{\lambda_G^{3+b_G}}, \end{aligned} \tag{A5}$$

whose assumption is that cloud water does not sediment and its size small enough to ignore comparing with the size of graupel. Performing integration using the formula $\Gamma(x)=\int_0^\infty t^{x-1}e^{-t}dt$ and dividing it by ρ to transform the unit from $\text{kgm}^{-3}\text{s}^{-1}$ to $\text{kgkg}^{-1}\text{s}^{-1}$, the accretion of cloud water by graupel can be expressed in a bulk formula as follows :

$$\begin{aligned} &\text{Pgacw}[\text{kgkg}^{-1}\text{s}^{-1}]\\ &=\frac{\pi a_G E_{GC} n_{0G} q_C}{4}\left(\frac{\rho_0}{\rho}\right)^{\frac{1}{2}}\frac{\Gamma(3+b_G)}{\lambda_G^{3+b_G}}. \end{aligned} \tag{A6}$$

The accretion of cloud water by snow to form graupel is similar to (A6), and is expressed as

$$\begin{aligned} &\text{Psacw}[\text{kgkg}^{-1}\text{s}^{-1}]\\ &=\frac{\pi a_S E_{SC} n_{0S} q_C}{4}\left(\frac{\rho_0}{\rho}\right)^{\frac{1}{2}}\frac{\Gamma(3+b_S)}{\lambda_S^{3+b_S}}, \end{aligned} \tag{A7}$$

where Pgacw and Psacw will contribute to form rain-

drop, if $T \geq T_0$.

The accretion of rain by snow is also assumed to follow the continuous collection equation, which can be expressed as

$$\int_0^\infty \frac{dM(D_S)}{dt} dD_S [\mathrm{kgm^{-3}s^{-1}}]$$

$$= \int_0^\infty \pi \left(\frac{D_S + D_R}{2} \right)^2 |V_S(D_S) - V_R(D_R)| E_{SR} \rho q_r n_S dD_S$$

$$= \int_0^\infty \int_0^\infty \pi \left(\frac{D_S + D_R}{2} \right)^2 |V_S(D_S) - V_R(D_R)|$$

$$\times E_{SR} \rho_W \frac{\pi}{6} D_R^3 n_R(D_R) dD_R n_S(D_S) dD_S . \qquad \text{(A8)}$$

With the assumption that the difference in the sedimentation velocity for snow and rain with respect to the diameter of snow can be neglected, the Eq. (A8) can be expressed as

$$= \frac{\pi^2 E_{SR} n_{0R} n_{0S} \rho_W}{24} |V_S(D_S) - V_R(D_R)|$$

$$\times \int_0^\infty \int_0^\infty (D_S + D_R)^2 D_R^3 \exp(-\lambda_R D_R) \exp(-\lambda_S D_S) dD_R dD_S$$

$$= \frac{\pi^2 E_{SR} n_{0R} n_{0S} \rho_W}{24} |V_S(D_S) - V_R(D_R)|$$

$$\times \int_0^\infty D_S^2 \frac{\Gamma(4)}{\lambda_R^4} + 2D_S \frac{\Gamma(5)}{\lambda_R^5} + \frac{\Gamma(6)}{\lambda_R^6} \exp(-\lambda_S D_S) dD_S$$

$$= \frac{\pi^2 E_{SR} n_{0R} n_{0S} \rho_W}{24} |V_S(D_S) - V_R(D_R)|$$

$$\times \left\{ \frac{\Gamma(4)}{\lambda_R^4} \frac{\Gamma(3)}{\lambda_S^3} + \frac{\Gamma(5)}{\lambda_R^5} \frac{2\Gamma(2)}{\lambda_R^2} + \frac{\Gamma(6)}{\lambda_R^6} \frac{\Gamma(1)}{\lambda_R^1} \right\}$$

$$= \frac{\pi^2 E_{SR} n_{0R} n_{0S} \rho_W}{24} |V_S(D_S) - V_R(D_R)|$$

$$\times \left\{ \frac{12}{\lambda_R^4 \lambda_S^3} + \frac{48}{\lambda_R^5 \lambda_S^2} + \frac{120}{\lambda_R^6 \lambda_S^1} \right\}, \qquad \text{(A9)}$$

dividing it by ρ to transform the unit from $\mathrm{kgm^{-3}s^{-1}}$ to $\mathrm{kgkg^{-1}s^{-1}}$, the accretion of rain by snow is given by

$$\mathrm{Psacr}[\mathrm{kgkg^{-1}s^{-1}}] = \pi^2 E_{SR} n_{0R} n_{0S} \left(\frac{\rho_W}{\rho} \right)$$

$$\times |V_S - V_R| \left(\frac{5}{\lambda_R^6 \lambda_S} + \frac{2}{\lambda_R^5 \lambda_S^2} + \frac{0.5}{\lambda_R^4 \lambda_S^3} \right), \qquad \text{(A10)}$$

where Pgacw and Psacr will contribute to the rain content if $T \geq T_0$. Similarly, the accretion of snow by rain is given as

$$\mathrm{Pracs}[\mathrm{kgkg^{-1}s^{-1}}] = \pi^2 E_{SR} n_{0R} n_{0S} \left(\frac{\rho_S}{\rho} \right)$$

$$\times |V_R - V_S| \left(\frac{5}{\lambda_S^6 \lambda_R} + \frac{2}{\lambda_S^5 \lambda_R^2} + \frac{0.5}{\lambda_S^4 \lambda_R^3} \right), \qquad \text{(A11)}$$

where Psacr and Pracs occur only when $T < T_0$.

Also, the accretion terms of rain (Pgacr) and snow (Pgacs) by graupel are of the form:

$$\mathrm{Pgacr}[\mathrm{kgkg^{-1}s^{-1}}] = \pi^2 E_{GR} n_{0G} n_{0R} \left(\frac{\rho_W}{\rho} \right)$$

$$\times |V_G - V_R| \left(\frac{5}{\lambda_R^6 \lambda_G} + \frac{2}{\lambda_R^5 \lambda_G^2} + \frac{0.5}{\lambda_R^4 \lambda_G^3} \right) \qquad \text{(A12)}$$

and

$$\mathrm{Pgacs}[\mathrm{kgkg^{-1}s^{-1}}] = \pi^2 E_{GS} n_{0S} n_{0G} \left(\frac{\rho_S}{\rho} \right)$$

$$\times |V_G - V_S| \left(\frac{5}{\lambda_S^6 \lambda_G} + \frac{2}{\lambda_S^5 \lambda_G^2} + \frac{0.5}{\lambda_S^4 \lambda_G^3} \right), \qquad \text{(A13)}$$

where Pgacr will contribute to Pgeml, if $T \geq T_0$.

The accretion terms, which consider the cloud ice falling velocity, are the processes of accretion of cloud ice by rain, snow, and graupel. The accretion of ice by rain is also assumed to follow the continuous collection equation:

$$\int_0^\infty \frac{dM(D_R)}{dt} dD_R [\mathrm{kgm^{-3}s^{-1}}]$$

$$= \int_0^\infty \pi \rho \left(\frac{D_R + D_I}{2} \right)^2 |V_R - V_I| \times q_I E_{RI} n_R(D_R) dD_R$$

$$= \frac{\pi q_I \rho E_{RI} n_{0R} |V_R - V_I|}{4} \times \int_0^\infty (D_R^2 + 2D_I D_R + D_I^2) \exp(-\lambda_R D_R) dD_R$$

$$= \frac{\pi q_I \rho E_{RI} n_{0R} |V_R - V_I|}{4} \times \left[\frac{\Gamma(3)}{\lambda_R^3} + 2D_I \times \frac{\Gamma(2)}{\lambda_R^2} + D_I^2 \times \frac{\Gamma(1)}{\lambda_R} \right]$$

$$= \frac{\pi q_I \rho E_{RI} n_{0R} |V_R - V_I|}{4} \times \left[2\lambda_R^{-3} + 2D_I \times \lambda_R^{-2} + D_I^2 \times \lambda_R^{-1} \right], \quad \text{(A14)}$$

dividing (A14) by ρ to transform the unit from $\mathrm{kgm^{-3}s^{-1}}$ to $\mathrm{kgkg^{-1}s^{-1}}$, the accretion of cloud ice by rain can be expressed as

$$\mathrm{Praci[kgkg^{-1}s^{-1}]} = \frac{\pi q_I E_{RI} n_{0R} |V_R - V_I|}{4} \times \left[2\lambda_R^{-3} + 2D_I \times \lambda_R^{-2} + D_I^2 \times \lambda_R^{-1} \right] \quad \text{(A15)}$$

and similarly other accretion terms are

$$\mathrm{Psaci[kgkg^{-1}s^{-1}]} = \frac{\pi q_I E_{SI} n_{0S} |V_S - V_I|}{4} \times \left[2\lambda_S^{-3} + 2D_I \times \lambda_S^{-2} + D_I^2 \times \lambda_S^{-1} \right] \quad \text{(A16)}$$

and

$$\mathrm{Pgaci[kgkg^{-1}s^{-1}]} = \frac{\pi q_I E_{GI} n_{0G} |V_G - V_I|}{4} \times \left[2\lambda_G^{-3} + 2D_I \times \lambda_G^{-2} + D_I^2 \times \lambda_G^{-1} \right]. \quad \text{(A17)}$$

These accretion terms, Pgaci and Praci, contribute to the growth of graupel, and Pgaci to the growth of snow, if $T < T_0$.

Graupel initiation by accretion of rain by cloud ice is obtained through multiplying the rate at which a cloud ice particle collides with raindrop (assumed to be uniformly distributed throughout the volume) by the number concentration of cloud ice. The collection of rain by cloud ice is also assumed to follow the continuous collection equation:

$$\int_0^\infty \frac{dM(D_R)}{dt} dD_R \ [\mathrm{kgm^{-3}s^{-1}}]$$

$$= \int_0^\infty \frac{\pi}{4} \rho D_R^2 V_R(D_R) q_I E_{RI} n_R(D_R) dD_R$$

$$= \int_0^\infty \frac{\pi}{4} \rho_W D_R^2 V_R(D_R) \frac{M_R}{\rho_R} N_I E_{RI} n_R(D_R) dD_R$$

$$= \frac{\pi^2}{24} a_R \rho_W E_{RI} n_{0R} N_I \left(\frac{\rho_0}{\rho} \right)^{\frac{1}{2}} \int_0^\infty D_R^{5+b_R} \exp(-\lambda_R D_R) dD_R$$

$$= \frac{\pi^2 a_R \rho_W E_{RI} n_{0R} N_I}{24} \left(\frac{\rho_0}{\rho} \right)^{\frac{1}{2}} \frac{\Gamma(6+b_R)}{\lambda_R^{6+b_R}}, \quad \text{(A18)}$$

dividing it by ρ to transform the unit from $\mathrm{kgm^{-3}s^{-1}}$ to $\mathrm{kgkg^{-1}s^{-1}}$, Piacr is given by

$$\mathrm{Piacr[kgkg^{-1}s^{-1}]} = \left[\int_0^\infty E_{RI} \frac{\pi}{4} D_R^2 V_R(D_R) \rho_W \times \frac{\pi}{6} D_R^3 n_R(D_R) dD_R \right] \times \frac{\rho q_I}{M_I} \times \left(\frac{1}{\rho} \right)$$

$$= \frac{\pi^2 a_R \rho_W E_{RI} n_{0R} N_I}{24\rho} \left(\frac{\rho_0}{\rho} \right)^{\frac{1}{2}} \frac{\Gamma(6+b_R)}{\lambda_R^{6+b_R}}. \quad \text{(A19)}$$

3) FREEZING (Pgfrz)

The equation for freezing of graupel, if $T < T_0$, can be expressed as

$$\mathrm{Pgfrz} = 20\pi^2 B' n_{0R} \left(\frac{\rho_W}{\rho} \right) \times \left\{ \exp\left[A'(T_0 - T) - 1 \right] \right\} \lambda_R^{-7}. \quad \text{(A20)}$$

4) DEPOSITION/SUBLIMATION (Pgdep)

Sublimation will occur in a subsaturated region (i.e. S_I -1<0, where S_I is saturation ratio over ice) and saturated region (i.e S_I -1>0). Pgdep is a production term for graupel as deposition ($T < T_0$), which can be expressed as

$$\mathrm{Pgdep[kgkg^{-1}s^{-1}]} = \int_0^\infty \frac{dM(D_G)}{dt} dD_G = \int_0^\infty \left[\frac{C(S_I - 1)/\varepsilon_0}{A_I + B_I} F \right] dD_G$$

$$= \frac{2\pi n_{0G}(S_I - 1)}{(A_I + B_I)} \left[\frac{0.78}{\lambda_G^2} + \frac{0.31\Gamma[(b_G+5)/2]}{\lambda_G^{(b_G+5)/2}} \times \left(\frac{\mu_K}{D} \right)^{\frac{1}{3}} \left(\frac{a_G}{\mu_K} \right)^{\frac{1}{2}} \left(\frac{\rho_0}{\rho} \right)^{\frac{1}{4}} \right], \quad \text{(A21)}$$

where $A_I = (L_S / K_a T)(L_S M_W / R^* T - 1)$ and $B_I = R^* T / D_f M_w e_{si}$.

5) MELTING (Pgmlt, Pgeml)

The graupel melted per unit volume is given by

$$\frac{dM(D_G)}{dt} = \frac{-2\pi}{L_f} K_a D_G (T - T_0) F. \quad \text{(A22)}$$

Integrating (A22) over the graupel size distribution, the melting rate, Pgmlt, if $T > T_0$, is obtained by

$$\text{Pgmlt[kgkg}^{-1}\text{s}^{-1}] = \frac{2\pi n_{0G} K_a (T - T_0)}{L_f} \left[\frac{0.78}{\lambda_G^2} + \frac{0.31\Gamma[(b_G+5)/2]}{\lambda_G^{(b_G+5)/2}} \times \left(\frac{\mu_K}{D} \right)^{1/3} \left(\frac{a_G}{\mu_K} \right)^{1/2} \left(\frac{\rho_0}{\rho} \right)^{1/4} \right]. \quad \text{(A23)}$$

The melting of graupel is enhanced by the accretion of cloud water and rain, if $T \geq T_0$, and can be expressed as

$$\text{Pgeml[kgkg}^{-1}\text{s}^{-1}] = \frac{-C_w}{L_f}(T - T_0)(\text{Pgacr} + \text{Pgacw}). \quad \text{(A24)}$$

6) EVAPORATION (Pgevp)

When graupel melts in air that is below water saturation and $T \geq T_0$, water can evaporate from the surface of graupel, which is given by

$$\text{Pgevp[kgkg}^{-1}\text{s}^{-1}] = \frac{2\pi n_{0G}(S_W - 1)}{(A_W + B_W)} \left[\frac{0.78}{\lambda_G^2} + \frac{0.31\Gamma[(b_G+5)/2]}{\lambda_G^{(b_G+5)/2}} \times \left(\frac{\mu_K}{D} \right)^{1/3} \left(\frac{a_G}{\mu_K} \right)^{1/2} \left(\frac{\rho_0}{\rho} \right)^{1/4} \right]. \quad \text{(A25)}$$

b. Production term for snow

The production term for snow may be written for two temperature regimes.

(i) If the temperature is below 0 °C ($T < T_0$):

$$S_S = \text{Psaut-Pgaut+Piacr}(\delta_3)\text{+Praci}(\delta_3)\text{+Psaci -Pgacs-Pracs}(1\text{-}\delta_2)\text{+Psacr}(\delta_2)\text{+Psdep}, \quad \text{(A26)}$$

where

$$\delta_2 = \begin{cases} 1, (q_R \text{ and } q_S < 10^{-4}\text{kgkg}^{-1}) \\ 0, \text{otherwise} \end{cases} \quad \text{(A27)}$$

and

$$\delta_3 = \begin{cases} 1, (q_R < 10^{-4}\text{kgkg}^{-1}) \\ 0, \text{otherwise}. \end{cases}$$

(ii) If the temperature is above 0 °C ($T \geq T_0$):

$$S_S = \text{-Pgacs+Psevp+Psmlt+Pseml}. \quad \text{(A28)}$$

1) AGGREGATION (Psaut)

The auto conversion (aggregation) rate of ice crystals to snow is given by

$$\text{Psaut[kgkg}^{-1}\text{s}^{-1}] = \max\left[(q_I - q_{Icrit}) / \Delta t, 0 \right], \quad \text{(A29)}$$

which occurs only for $T < T_0$. Pgaut is obtained by Eq. (A4). This term has negative contribution to snow, if $T < T_0$.

2) ACCRETION (Psaci, Piacr, Praci, Pgacs, Pracs, Psacr)

The impact of accretion process of cloud ice by snow is stronger than other processes. As in (A14), the accretion term considering the sedimentation of cloud ice can be expressed as

$$\text{Psaci}[\text{kgkg}^{-1}\text{s}^{-1}] = \frac{\pi q_I E_{SI} n_{0S} |V_S - V_I|}{4} \times 2 \times \left[\lambda_S^{-3} + 2D_I \times \lambda_S^{-2} + D_I^2 \times \lambda_S^{-1}\right]. \quad \text{(A30)}$$

Other accretion terms to form snow, Piacr and Praci, are given earlier by (A19) and (A15), respectively. A threshold for the rainwater content to determine whether the interaction of rain and cloud ice results in snow or graupel is based on Lin *et al.* (1983).

3) DEPOSITION/SUBLIMATION (Psdep)

The continuous growth equation for snow, if $T < T_0$, is given by

$$\text{Psdep}[\text{kgkg}^{-1}\text{s}^{-1}] = \frac{4n_{0S}(S_I - 1)}{(A_I + B_I)} \times \left[\frac{0.65}{\lambda_S^2} + \frac{0.44\Gamma[(b_S+5)/2]}{\lambda_S^{(b_S+5)/2}} \times \left(\frac{\mu_K}{D}\right)^{1/3} \left(\frac{a_S \rho}{\mu_K}\right)^{1/2} \left(\frac{\rho_0}{\rho}\right)^{1/4} \frac{\Gamma[(b_S+5)/2]}{\lambda_S^{(b_S+5)/2}}\right]. \quad \text{(A31)}$$

Compared to the process with $n_{0S}=2\times10^7\text{m}^{-4}$ in Rutledge and Hobbs (1983) and Dudhia (1989), the formula for n_{0S} in HDC produces larger (smaller) Psdep at colder (warmer) temperatures, consistent with the assumed broadening of the snow size spectrum.

4) MELTING (Psmlt, Pseml)

The snow melted per unit time is given by

$$\frac{dM(D_s)}{dt} = \frac{-2\pi}{L_f} K_a D_s (T - T_0) F \quad \text{(A32)}$$

and then multiplying size distribution, and integrating over all snow sizes we obtain the melting of snow, if $T > T_0$, and is expressed as

$$\text{Psmlt}[\text{kgkg}^{-1}\text{s}^{-1}] = \frac{2\pi n_{0S}}{L_f} K_a (T - T_0) \left[\frac{0.65}{\lambda_S^2} + \frac{0.44\Gamma[(b_S+5)/2]}{\lambda_S^{(5+b_S)/2}} \times \left(\frac{\mu_K}{D}\right)^{1/3} \left(\frac{a_S}{\mu_K}\right)^{1/2} \left(\frac{\rho_0}{\rho}\right)^{1/4}\right]. \quad \text{(A33)}$$

The melting of snow is enhanced by the accretion of cloud water and rain, if $T \geq T_0$, and is expressed as

$$\text{Pseml}[\text{kgkg}^{-1}\text{s}^{-1}] = \frac{-C_W}{L_f}(T - T_0)(\text{Psacr} + \text{Psacw}). \quad \text{(A34)}$$

5) EVAPORATION (Psevp)

By Rutledge and Hobbs (1983), evaporation is from a liquid surface, if $T \geq T_0$, and is expressed as

$$\text{Psevp}[\text{kgkg}^{-1}\text{s}^{-1}] = \frac{4n_{0S}(S_W - 1)}{(A_W + B_W)} \times \left[\frac{0.65}{\lambda_S^2} + \frac{0.44\Gamma[(b_S+5)/2]}{\lambda_S^{(b_S+5)/2}} \times \left(\frac{\mu_K}{D}\right)^{1/3} \left(\frac{a_S \rho}{\mu_K}\right)^{1/2} \left(\frac{\rho_0}{\rho}\right)^{1/2} \frac{\Gamma[(b_S+5)/2]}{\lambda_S^{(b_S+5)/2}}\right]. \quad \text{(A35)}$$

c. Production term for rain

The production term for rain may be written for two temperature regimes.

(i) If the temperature is below 0 °C ($T < T_0$):

$$S_R = \text{Praut} + \text{Pracw} - \text{Piacr} - \text{Pgacr} - \text{Psacr} - \text{Pfrz} + \text{Prevp}. \quad \text{(A36)}$$

(ii) If the temperature is above 0 °C ($T \geq T_0$):

$$S_R = \text{Praut} + \text{Psacw} + \text{Pracw} + \text{Pgacw} + \text{Prevp} - \text{Psmlt} - \text{Pseml} - \text{Pgmlt} - \text{Pgeml}. \quad \text{(A37)}$$

1) AUTOCONVERSION (Praut)

HDC adapted the auto conversion parameterization with a stronger physical basis (Tripoli and

Cotton 1980) and can be expressed as

$$\text{Praut}[\text{kgkg}^{-1}\text{s}^{-1}] = \frac{0.104 g E_C \rho_0^{4/3}}{\mu (N_C \rho_W)^{1/3}} \times q_C^{7/3} H(q_C - q_{C0}), \quad \text{(A38)}$$

where $H(x)$ is the Heaviside unit step function, which suppresses the auto conversion processes until cloud water reaches a critical mixing ratio (q_{C0}),

$$q_{C0}(\text{kg kg}^{-1}) = \frac{4\pi \rho_w r_{cr}^3 N_C}{3\rho}, \quad \text{(A39)}$$

where r_{cr} is the critical mean droplet radius at which the auto conversion begins.

2) ACCRETION (Pracw, Psacw, Pgacw, Psacr, Pgacr, Piacr)

By applying the geometric sweep-out concept and integrating over all raindrop sizes, as in (A5) the grow rate of raindrop by accretion of cloud water is given by

$$\text{Pracw}[\text{kgkg}^{-1}\text{s}^{-1}] = \frac{\pi a_R E_{RC} n_{0R} q_C}{4} \times \left(\frac{\rho_0}{\rho}\right)^{\frac{1}{2}} \frac{\Gamma(3+b_R)}{\lambda_R^{3+b_R}}. \quad \text{(A40)}$$

In the temperature region, $T < T_0$, there are three additional accretion terms of Psacr, Pgacr and Piacr, which provide negative contributions to the rain field. Two other accretion processes, Psacw and Pgacw, provide positive contribution to rain, if $T \geq T_0$. Psacw and Pgacw are given earlier by (A7) and (A6), respectively.

Psacr, Pgacr, and Piacr are also given by (A10), (A12), and (A19), respectively.

3) FREEZING (Pgfrz)

Pgfrz is obtained by (A20).

4) EVAPORATION / CONDENSATION (Prevp)

As in Rutledge and Hobbs (1983) and Dudhia (1989), the continuous growth equation of raindrop is given by

$$\text{Prevp}[\text{kgkg}^{-1}\text{s}^{-1}] = \frac{2\pi n_{0R}(S_W - 1)}{(A_W + B_W)} \times \left[\frac{0.78}{\lambda_R^2} + \frac{0.31\Gamma[(b_R+5)/2]}{\lambda_R^{(b_R+5)/2}} \times \left(\frac{\mu_K}{D}\right)\left(\frac{a_R \rho}{\mu_K}\right)^{1/2}\left(\frac{\rho_0}{\rho}\right)^{1/4}\right]. \quad \text{(A41)}$$

5) MELTING (Psmlt, Pseml, Pgmlt, Pgeml)

Psmlt and Pseml are given by (A32) and (A33), and Pgmlt and Pgeml are same as (A22) and (A23), respectively.

d. Production term for cloud water

The production term for cloud water may be written for two temperature regimes.

(i) If the temperature is below 0 °C ($T < T_0$):

$$S_C = -\text{Praut} - \text{Pracw} - \text{Psacw} - \text{Pgacw} + \text{Pcond} - \text{Pihtf} - \text{Pihmf}. \quad \text{(A42)}$$

(ii) If the temperature is above 0 °C ($T \geq T_0$):

$$S_C = -\text{Praut} - \text{Pracw} - \text{Psacw} - \text{Pgacw} + \text{Pimlt}. \quad \text{(A43)}$$

1) AGGREGATION (Praut)

Praut is obtained by (A37).

2) ACCRETION (Pracw, Psacw, Pgacw)

Pracw, Psacw, and Pgacw are given, respectively, by (A40),(A7) and (A6).

3) FREEZING (Pihtf, Pihmf)

Following Biggs (1953), Pihtf (heterogeneous freezing of cloud water) will occur when -40 °C < T < T_0, which can be expressed as

$$\text{Pihtf}[\text{kgkg}^{-1}\text{s}^{-1}]$$

$$= B'[\exp\{A'(T_0 - T')\} - 1]\frac{\rho q_c^2}{\rho_W N_C}. \quad \text{(A44)}$$

This term represents another source term of cloud water to ice. Also, Pihmf (homogeneous freezing of cloud water) serves as source term for cloud ice when the temperature is below -40 °C.

$$\text{Pihmf}[\text{kgkg}^{-1}\text{s}^{-1}] = \rho q_C / \Delta t \quad \text{(A45)}$$

4) CONDENSATION /EVAPORATION (Pcond)

Following Yau and Austin (1979), we express the condensation of water vapor to cloud water as

$$\text{Pcond}[\text{kgkg}^{-1}\text{s}^{-1}] = (q - q_{SW}) \times \left[\Delta t\left(1 + \frac{L_v^2 q_{SW}}{C_{pm} R_V T^2}\right)\right]^{-1}, \quad \text{(A46)}$$

where cloud water evaporates, if $q < q_{SW}$.

5) MELTING (Pimlt)

Melting of cloud ice to form cloud water is assumed to occur instantaneously, if $T \geq T_0$, and is given by

$$\text{Pimlt}[\text{kgkg}^{-1}\text{s}^{-1}] = \rho q_I / \Delta t. \quad \text{(A47)}$$

e. Production term for cloud ice

The production term for cloud ice may be written for two temperature regimes.

(i) If the temperature is below 0 °C ($T < T_0$):

$$S_I = \text{-Psaut-Praci-Psaci-Pgaci+Pigen +Pidep+Pihtf+Pihmf}. \quad \text{(A48)}$$

(ii) If the temperature is below 0 °C ($T \geq T_0$):

$$S_I = \text{-Pimlt}. \quad \text{(A49)}$$

1) Initiation of cloud ice crystal (Pigen)

For Rutledge and Hobbs (1983) and Dudhia (1989), the initiation rate of cloud ice from water vapor when $T < T_0$ and the air is supersaturated with respect to ice under the no ice condition, is given by

$$\text{Pigen}[\text{kgkg}^{-1}\text{s}^{-1}] = \min\left[(q_{I0} - q_I)/\Delta t, (q - q_{SI})/\Delta t\right], \quad \text{(A50)}$$

where Pigen ≥ 0. HDC treats the ice crystal number concentration (N_I) separately from the ice nuclei number concentration (N_{I0}).

2) AGGREGATION (Psaut)

Psaut is presented by (A29).

3) ACCRETION (Praci, Psaci, Pgaci)

Praci, Psaci and Pgaci are given by (A15), (A16), and (A17).

4) FREEZING (Pihtf, Pihmf)

Pihtf and Pihmf are source terms for cloud ice, as given by (A44) and (A45).

5) DEPOSITION/SUBLIMATION (Pidep)

For HDC, the growth (dissipation) rate of ice crystals by deposition of water vapor (sublimation of ice), when the air is supersaturated (subsaturated) with respect to ice, which is given by

$$\text{Pidep}[\text{kgkg}^{-1}\text{s}^{-1}] = \frac{4\bar{D}_I(S_I - 1)N_I}{A_I + B_I}. \quad \text{(A51)}$$

Due to the HDC's formulation of N_I that generally implies larger crystals, Pidep is slower at colder temperatures, as it should be, whereas Pidep was unrealistically active at colder temperatures in Rutledge and Hobbs (1983). HDC's formula for Pigen is more active at colder temperatures than Pidep, which is more active at warmer temperatures.

6) MELTING (Pgeml, Pseml, Pimlt)

Pgeml, Pseml, and Pimlt are given by (A24), (A34), and (A47), respectively.

Appendix B. List of Symbols

Symbol	Description	Value	SI units
A'	Constant in Biggs freezing	0.66	K^{-1}
A_I	Thermodynamic term	$(L_S / K_a T)(L_S M_W / R^* T - 1)$	$mskg^{-1}$
A_W	Thermodynamic term	$(L_v / K_a T)(L_v M_w / R^* T - 1)$	$mskg^{-1}$
a_G	Empirical formula of V_G	330	$m^{1-b}s^{-1}$
a_R	Empirical formula of V_R	841.9	$m^{1-b}s^{-1}$
a_S	Empirical formula of V_S	11.72	$m^{1-b}s^{-1}$
B'	Constant in rain drop freezing equation	100	$m^{-3}\ s^{-1}$
B_I	Thermodynamic term	$R^* T / D_f M_w e_{si}$	$mskg^{-1}$
B_W	Thermodynamic term	$R^* T / D_f M_w e_{sw}$	$mskg^{-1}$
b_G	Empirical formula of V_R	0.8	
b_R	Empirical formula of V_G	0.8	
b_S	Empirical formula of V_S	0.41	
C	Capacitance of ice crystal	$2\pi\varepsilon_0 D_G$	$C^2N^{-1}\ m^{-1}$
C_{pd}	Specific heat of dry air at constant pressure	1005.7	$Jkg^{-1}K^{-1}$
C_{pm}	Specific heat of most air at constant pressure	$C_{pd}(1-q)+q(C_{pv})$	$Jkg^{-1}K^{-1}$
C_{pv}	Specific heat of water vapor at constant pressure	1870	$Jkg^{-1}K^{-1}$
C_W	Specific heat of liquid water	4190	$Jkg^{-1}K^{-1}$
D	Diffusion coefficient of the water vapor	$8.794\times10^{-5}\times T^{1.81}/P$	$m^2\ s^{-1}$
D_f	Diffusivity of water vapor in air	2.26×10^{-5}	$m^2\ s^{-1}$
D_G	Graupel diameter		m
D_R	Rain diameter		m
D_I	Cloud ice diameter		m
$\overline{D}_I$	Cloud ice diameter defined in HDC	HDC(5b)	m
D_S	Snow diameter		m
E_C	Mean collection efficiency	0.55	
E_{GC}	Graupel/cloud water collection efficiency	1	
E_{GI}	Graupel/cloud ice collection efficiency	$\exp[0.07(T-T_0)]$	
E_{GR}	Graupel/rain collection efficiency	1	
E_{GS}	Graupel/snow collection efficiency	1, $T \geq 0$ $\exp[0.09(T-T_0)]$, $T<0$	
E_{RC}	Rain/cloud water collection efficiency	1	
E_{RI}	Rain/cloud ice collection efficiency	1	
E_{SC}	Snow/cloud water collection efficiency	1	
E_{SI}	Snow/cloud ice collection efficiency	$\exp[0.07(T-T_0)]$	
E_{SR}	Snow/rain collection efficiency	1	
e_{si}	Saturation vapor pressure for ice		$kgm^{-1}s^{-2}$
e_{sw}	Saturation vapor pressure for water		$kgm^{-1}s^{-2}$
F	Ventilation factor	$0.78+0.31S_c^{1/3}R_e^{1/2}$, $T \geq 0$ $0.65+0.44S_c^{1/3}R_e^{1/2}$, $T<0$	
g	Gravitational acceleration	9.8	ms^{-2}
K_a	Thermal conductivity of air	2.43×10^{-2}	$Jm^{-1}s^{-1}K^{-1}$
L_f	Latent heat of fusion	3.34×10^5	Jkg^{-1}
L_S	Latent heat of sublimation	2.5×10^6	Jkg^{-1}
L_V	Latent heat of condensation	2.25×10^6	Jkg^{-1}
$M(D_G)$	Mass of graupel of diameter D_G		kg

$M(D_I)$	Mass of ice crystal of diameter D_I		kg
$M(D_R)$	Mass of rain of diameter D_R		kg
$M(D_S)$	Mass of snowflake of diameter D_S		kg
M_I	Average mass of a cloud ice crystal	6×10^{-12}	kg
M_{I0}	Average mass of a cloud ice nuclei	10^{-12}	kg
M_W	Molecular weight of water	18.0160	
N_c	Number concentration of cloud water droplet	3×10^{8}	m^{-3}
$n_G(D_G)$	Number concentration of graupel of diameter D_G		m^{-3}
N_I	Number concentration of ice crystal	HDC(5c)	m^{-3}
N_{I0}	Number concentration of ice nuclei	HDC(8)	m^{-3}
$n_R(D_R)$	Number concentration of rain of diameter D_R		m^{-3}
$n_S(D_S)$	Number concentration of snow of diameter D_S		m^{-3}
n_{0G}	Intercept parameter of graupel	4×10^{6}	m^{-4}
n_{0R}	Intercept parameter of rain	8×10^{6}	m^{-4}
n_{0S}	Intercept parameter of snow	$2\times10^{6}\exp\left[0.12(T-T_0)\right]$	m^{-4}
$n_G dD_G$	Number concentration of snowflakes with diameters between D_G and D_G+dD_G		m^{-3}
$n_R dD_R$	Number concentration of raindrops with diameters between D_R and D_R+dD_R		m^{-3}
$n_S dD_S$	Number concentration of snowflakes with diameters between D_S and D_S+dD_S		m^{-3}
Pgaci	Production rate for accretion of cloud ice by graupel		$kgkg^{-1}s^{-1}$
Pgacw	Production rate for accretion of cloud water by graupel		$kgkg^{-1}s^{-1}$
Pgacr	Production rate for accretion of rain by graupel		$kgkg^{-1}s^{-1}$
Pgacs	Production rate for accretion of snow by graupel		$kgkg^{-1}s^{-1}$
Psaci	Production rate for accretion of cloud ice by snow		$kgkg^{-1}s^{-1}$
Psacw	Production rate for accretion of cloud water by snow		$kgkg^{-1}s^{-1}$
Pracs	Production rate for accretion of snow by rain		$kgkg^{-1}s^{-1}$
Psacr	Production rate for accretion of rain by snow		$kgkg^{-1}s^{-1}$
Praci	Production rate for accretion of cloud ice by rain		$kgkg^{-1}s^{-1}$
Piacr	Production rate for accretion of rain by cloud ice		$kgkg^{-1}s^{-1}$
Pracw	Production rate for accretion of cloud water by rain		$kgkg^{-1}s^{-1}$
Pgmlt	Production rate for melting of cloud ice to form cloud water		$kgkg^{-1}s^{-1}$
Pgeml	Production rate induced by enhanced melting rate of graupel		$kgkg^{-1}s^{-1}$
Psmlt	Production rate for melting of melting of snow to form cloud water		$kgkg^{-1}s^{-1}$
Pseml	Production rate induced by enhanced melting of snow		$kgkg^{-1}s^{-1}$
Prevp	Production rate for evaporation/condensation rate of rain		$kgkg^{-1}s^{-1}$
Psdep	Production rate for deposition/sublimation rate of snow		$kgkg^{-1}s^{-1}$
Pgdep	Production rate for deposition/sublimation rate of graupel		$kgkg^{-1}s^{-1}$
Praut	Production rate for auto conversion of cloud water to form rain		$kgkg^{-1}s^{-1}$
Psaut	Production rate for auto conversion of cloud ice to form snow		$kgkg^{-1}s^{-1}$
Pgaut	Production rate for auto conversion of snow to form graupel		$kgkg^{-1}s^{-1}$
Pgevp	Production rate for evaporation of melting graupel		$kgkg^{-1}s^{-1}$
Psevp	Production rate for evaporation of melting snow		$kgkg^{-1}s^{-1}$
Pcond	Production rate for condensation/ evaporation of cloud water		$kgkg^{-1}s^{-1}$
Pgfrz	Production rate for freezing of rain water to graupel		$kgkg^{-1}s^{-1}$
Pimlt	Production rate for instantaneous melting of cloud ice		$kgkg^{-1}s^{-1}$
Pihmf	Production rate for Homogeneous freezing of cloud water to form cloud ice		$kgkg^{-1}s^{-1}$
Pihtf	Production rate for heterogeneous freezing of cloud water to form cloud ice		$kgkg^{-1}s^{-1}$

Pidep	Production rate for deposition/sublimation rate of ice		$kgkg^{-1}s^{-1}$
Pigen	Production rate for generation(nucleation) of ice from vapor		$kgkg^{-1}s^{-1}$
q	Mixing ratio of water vapor		$kgkg^{-1}$
q_C	Mixing ratio of cloud water		$kgkg^{-1}$
q_{C0}	Critical mixing ratio of cloud water		$kgkg^{-1}$
q_G	Mixing ratio of graupel		$kgkg^{-1}$
q_I	Mixing ratio of ice crystal		$kgkg^{-1}$
q_{Icrit}	Critical mixing ratio of ice crystal	HDC (13)	$kgkg^{-1}$
q_{I0}	Mixing ratio of ice nuclei		$kgkg^{-1}$
q_R	Mixing ratio of rain		$kgkg^{-1}$
q_S	Mixing ratio of snow		$kgkg^{-1}$
q_{SI}	Saturated value with respect to ice		$kgkg^{-1}$
q_{SW}	Saturated value with respect to cloud water		$kgkg^{-1}$
q_{S0}	Threshold amount for aggregation to occur		$kgkg^{-1}$
R^*	Universal gas constant	8.314×10^{3}	$Jkmol^{-1}K^{-1}$
R_V	Gas constant for water vapor	4.61×10^{2}	$Jkg^{-1}K^{-1}$
R_e	Reynolds number		
r_{cr}	Critical mean droplet radius at which auto conversion begins	8×10^{-6}	m
S_C	Schmidt number	0.6	
	Sum of production rate for cloud water		$kgkg^{-1}s^{-1}$
S_G	Sum of production rate for graupel		$kgkg^{-1}s^{-1}$
S_I	Saturation ratio over ice		
	Sum of production rate for snow		$kgkg^{-1}s^{-1}$
S_R	Sum of production rate for rain		$kgkg^{-1}s^{-1}$
S_S	Sum of production rate for snow		$kgkg^{-1}s^{-1}$
S_W	Saturation ratio with respect to water		
T	Temperature		K
T_0	Reference Temperature	273.16	K
V_G	Mass weighted fall speed of graupel		ms^{-1}
V_I	Mass weighted fall speed of cloud ice		ms^{-1}
V_R	Mass weighted fall speed of rain		ms^{-1}
V_S	Mass weighted fall speed of snow		ms^{-1}
$V_G(D_G)$	Fall speed of snowflakes of diameter D_G		ms^{-1}
$V_R(D_R)$	Fall speed of snowflakes of diameter D_R		ms^{-1}
$V_S(D_S)$	Fall speed of snowflakes of diameter D_S		ms^{-1}
$V_I(D_I)$	Fall speed of snowflakes of diameter D_I	HDC(5a)	ms^{-1}
α_2	Parameter of the aggregation efficiency	$10^{-3}\exp[0.09(T-T_0)]$	
ρ	Air density		kgm^{-3}
ρ_G	Density of graupel	500	kgm^{-3}
ρ_S	Density of snow	100	kgm^{-3}
ρ_W	Density of water	10^{3}	kgm^{-3}
ρ_0	Density of air at reference state	1.28	kgm^{-3}
Δt	Time step for cloud microphysics		s
λ_G	Slope of graupel size distribution		m^{-1}
λ_R	Slope of rain size distribution		m^{-1}
λ_S	Slope of snow size distribution		m^{-1}
μ	Dynamic viscosity of air	1.718×10^{-5}	$gm^{-1}s^{-1}$
μ_K	Kinematic viscosity		m^2s^{-1}
ε_0	Permittivity of free space	8.854×10^{-12}	$C^2N^{-1}m^{-2}$